J. Fluid Mech. (2002), *vol.* 472, *pp.* 399–410. © 2002 Cambridge University Press
DOI: 10.1017/S0022112002002409 Printed in the United Kingdom

Hydromagnetic Taylor–Couette flow: wavy modes

By A. P. WILLIS AND C. F. BARENGHI
Department of Mathematics, University of Newcastle, Newcastle NE1 7RU, UK

(Received 25 March 2002 and in revised form 14 July 2002)

We investigate magnetic Taylor–Couette flow in the presence of an imposed axial magnetic field. First we calculate nonlinear steady axisymmetric solutions and determine how their strength depends on the applied magnetic field. Then we perturb these solutions to find the critical Reynolds numbers for the appearance of wavy modes, and the related wave speeds, at increasing magnetic field strength. We find that values of imposed magnetic field which alter only slightly the transition from circular-Couette flow to Taylor-vortex flow, can shift the transition from Taylor-vortex flow to wavy modes by a substantial amount. The results are compared to those for onset in the absence of a magnetic field.

1. Introduction

Taylor–Couette flow is one of the most important examples of fluid systems that exhibits the spontaneous formation of increasingly complex dynamic flow structures. This occurs through a sequence of transitions which take place as the drive is increased (Andereck, Liu & Swinney 1986). The first transition takes place when circular-Couette flow (CCF) becomes unstable to axisymmetric disturbances which grow into a toroidal flow pattern (Taylor-vortex flow – TVF). The second transition occurs when the Taylor vortices become unstable to non-axisymmetric perturbations, which results in a variety of time-dependent flows (wavy modes). More transitions take place at higher Reynolds numbers and a great number of variations of the original pattern observed by Taylor (1923) have been investigated (Egbers & Pfister 2000).

Our concern is Taylor–Couette flow in the presence of an axially imposed magnetic field. Despite early theoretical (Chandrasekhar 1961) and experimental interest (Donnelly & Ozima 1962), this case has been much less studied. The success of recent dynamo experiments (Gailitis *et al.* 2001; Stieglitz & Müller 2001) and the astrophysical interest in the magneto-rotational instability (Ji *et al.* 2001; Rüdiger & Zhang 2001) add further motivation.

In our previous paper (Willis & Barenghi 2002) we presented a convenient numerical formulation of the hydromagnetic Taylor–Couette flow problem. We determined critical Reynolds numbers for the appearance of axisymmetric Taylor vortices, calculated finite-amplitude solutions and compared our results with existing theoretical work and experiments. The aim of this paper is to continue this investigation into the three-dimensional time-dependent flow regime of the wavy modes.

2. Formulation and method of solution

Throughout this work we shall use the same notation as that of our previous paper. The fluid is contained between two concentric cylinders of inner radius R_1

https://doi.org/10.1017/S0022112002002409 Published online by Cambridge University Press

and outer radius R_2 which rotate at constant angular velocity Ω_1 and Ω_2 respectively. We make the usual assumption that the cylinders have infinite height, use cylindrical coordinates (r, θ, z), and assume that a constant magnetic field $\boldsymbol{B}_0 = \mu_0 H \hat{\boldsymbol{z}}$ is applied externally in the axial direction.

We introduce the following dimensionless parameters: radius ratio (η), Reynolds numbers (Re_1 and Re_2), Hartmann number (Q) and magnetic Prandtl number (ξ) defined as

$$\eta = R_1/R_2, \quad Re_i = \frac{R_i \Omega_i \delta}{\nu} \ (i = 1, 2), \quad Q = \frac{\mu_0^2 H^2 \sigma \delta^2}{\rho \nu}, \quad \xi = \frac{\nu}{\lambda}, \tag{2.1}$$

where δ is the gap width, ρ the density, ν the kinematic viscosity, λ the magnetic diffusivity and μ_0 the magnetic permeability. Hereafter we assume that ρ, ν, λ and μ_0 are constant.

The dimensionless equations governing incompressible hydromagnetic flow are

$$\partial_t \boldsymbol{u} + (\boldsymbol{u} \cdot \nabla)\boldsymbol{u} = -\nabla p + \nabla^2 \boldsymbol{u} + \frac{Q}{\xi}(\nabla \wedge \boldsymbol{B}) \wedge \boldsymbol{B}, \qquad \nabla \cdot \boldsymbol{u} = 0, \tag{2.2a,b}$$

$$\partial_t \boldsymbol{B} = \frac{1}{\xi}\nabla^2 \boldsymbol{B} + \nabla \wedge (\boldsymbol{u} \wedge \boldsymbol{B}), \qquad \nabla \cdot \boldsymbol{B} = 0. \tag{2.2c,d}$$

These equations have as a steady-state solution, $\tilde{\boldsymbol{u}}$, the circular-Couette flow, where

$$\tilde{u}_r = \tilde{u}_z = 0, \qquad \tilde{u}_\theta = Ar + B/r. \tag{2.3}$$

The constants A and B are determined by the no-slip boundary conditions.

Boundary conditions for the magnetic field can have a major influence on the flow, as found by Hollerbach & Skinner (2001) when studying the analogous problem in spherical geometry. Here the axially imposed magnetic field does not penetrate the boundaries but there are still differences with the theoretical results of Chandrasekhar (1961) for insulating and perfectly conducting cylinders. However, in experiments by Donnelly & Ozima (1962) using mercury, only a small difference was found between results with Perspex and stainless-steel containers. Therefore for practical reasons we take insulating boundary conditions for the magnetic field. If the magnetic field is expanded over modes of the form

$$\boldsymbol{B}(r, \theta, z) = \boldsymbol{B}(r)\, \mathrm{e}^{\mathrm{i}(\alpha z + m\theta)}, \tag{2.4}$$

then the boundary conditions are

$$\alpha = m = 0\text{:} \ \ B_\theta = B_z = 0; \tag{2.5a}$$

$$\alpha = 0, m \neq 0\text{:} \ \ \partial_\theta B_r = \pm m B_\theta, \quad B_z = 0; \tag{2.5b}$$

$$\alpha \neq 0\text{:} \ \ \partial_z B_r = \frac{\partial_r \mathscr{B}_m}{\mathscr{B}_m} B_z, \quad \frac{1}{r}\partial_\theta B_z = \partial_z B_\theta. \tag{2.5c}$$

The function $\mathscr{B}_m(r)$ denotes the modified Bessel functions $I_m(\alpha r)$ and $K_m(\alpha r)$, and the boundary condition (2.5*a–c*) is evaluated at R_1 and R_2 respectively, where for $\pm$ we take $+$ at R_1 and $-$ at R_2.

The magnetic Prandtl number, ξ, is very small in liquid metals available in the laboratory (mercury, $\xi = 0.145 \times 10^{-6}$; liquid sodium at 120 °C, $\xi = 0.89 \times 10^{-5}$). We set

$$\boldsymbol{B} = \boldsymbol{B}_0 + \xi \boldsymbol{b}, \tag{2.6}$$

where $\boldsymbol{B}_0$ is an externally applied field. In the limit $\xi \to 0$ the equations governing

https://doi.org/10.1017/S0022112002002409 Published online by Cambridge University Press

the disturbance to the circular-Couette flow become

$$(\partial_t - \nabla^2)\boldsymbol{u}' = \boldsymbol{N} - \nabla p', \qquad \nabla \cdot \boldsymbol{u}' = 0, \tag{2.7a,b}$$

$$\nabla^2 \boldsymbol{b} = \boldsymbol{N}_B, \qquad \nabla \cdot \boldsymbol{b} = 0, \tag{2.7c,d}$$

where

$$\boldsymbol{N} = Q(\nabla \wedge \boldsymbol{b}) \wedge \boldsymbol{B}_0 - (\boldsymbol{u} \cdot \nabla)\boldsymbol{u}' - (\boldsymbol{u}' \cdot \nabla)\tilde{\boldsymbol{u}}, \qquad \boldsymbol{N}_B = -\nabla \wedge (\boldsymbol{u} \wedge \boldsymbol{B}_0). \tag{2.7e,f}$$

The finite-amplitude disturbance $\boldsymbol{u}' = \boldsymbol{u} - \tilde{\boldsymbol{u}}$ satisfies homogeneous Dirichlet boundary conditions. The magnetic field $\boldsymbol{b}$ satisfies the same boundary conditions as $\boldsymbol{B}$ and is completely defined by the velocity at any particular time.

The method of solution of (2.7*a–d*) was the topic of our earlier paper, Willis & Barenghi (2002), which contains further details, including tests of the numerical method and comparison with calculations performed by others. Here it suffices to say that to ensure divergence-free fields we adopt the toroidal–poloidal decomposition

$$\boldsymbol{A} = \psi_0 \hat{\boldsymbol{\theta}} + \phi_0 \hat{\boldsymbol{z}} + \nabla \wedge (\psi \boldsymbol{r}) + \nabla \wedge \nabla \wedge (\phi \boldsymbol{r}), \tag{2.8}$$

where $\psi(r,t,z)$, $\phi(r,t,z)$ and $\psi_0(r)$, $\phi_0(r)$ contain the periodic and non-periodic parts of the field respectively. The potentials ψ, ϕ are expanded over Fourier modes in the periodic coordinates and Chebyshev polynomials in the radial direction.

The governing equations for the magnetic field are the r-components of the induction equation and its first curl. Although it is common to take the first and second curls for the velocity, we follow the procedure applied to the magnetic field and take the r-components of the momentum equation and its first curl. As the pressure has not been eliminated, we also take the divergence to obtain the pressure-Poisson equation.

Whilst the decomposition (2.8) raises the order of the equations, the extra derivatives appear in the periodic coordinates, so no extra boundary conditions are required. All five governing equations are second order in r. This property makes them easy to timestep stably and accurately, even for fully nonlinear three-dimensional flows, and simplifies implementation a great deal.

The equations are collocated in the radial direction and the nonlinear terms (2.7*e*, *f*) are evaluated pseudo-spectrally where necessary. Explicit Adams–Bashforth timestepping is used on the nonlinear terms and implicit Crank–Nicolson on the linear terms.

3. An imposed axial field

The equation defining the magnetic field, (2.7*c*), may be re-written as

$$\nabla \wedge \nabla \wedge \boldsymbol{b} = \nabla \wedge (\boldsymbol{u}' \wedge \hat{\boldsymbol{z}}), \tag{3.1}$$

since $\nabla \wedge (\tilde{\boldsymbol{u}} \wedge \hat{\boldsymbol{z}}) = \boldsymbol{0}$. Equation (3.1) can be integrated immediately to obtain

$$\nabla \wedge \boldsymbol{b} = (\boldsymbol{u}' \wedge \hat{\boldsymbol{z}}) - \nabla \Psi, \tag{3.2}$$

where, by taking the divergence, Ψ solves

$$\left.\begin{array}{lll} \nabla^2 \Psi = \omega_z' & \text{for} & R_1 < r < R_2, \\ \partial_r \Psi = 0 & \text{on} & r = R_1, R_2, \end{array}\right\} \tag{3.3}$$

and ω_z' is the z-component of vorticity. The function Ψ is related to the z-component

https://doi.org/10.1017/S0022112002002409 Published online by Cambridge University Press

of the streamfunction, $\boldsymbol{\Phi}$, for three-dimensional incompressible flow ($\boldsymbol{u} = \nabla \wedge \boldsymbol{\Phi}$; $\boldsymbol{\omega} = -\nabla^2 \boldsymbol{\Phi}$). The boundary conditions for $\boldsymbol{\Phi}$ are determined by the no-slip condition. Here, Ψ satisfies the homogeneous Neumann boundary condition that there be no current through the boundaries, $\hat{\boldsymbol{r}} \cdot \nabla \wedge \boldsymbol{b} = 0$. The following analysis may differ slightly for non-insulating boundaries.

The effect of the magnetic field on the fluid is introduced via the Lorentz force, which can now be written as

$$\boldsymbol{L} = Q(\nabla \wedge \boldsymbol{b}) \wedge \hat{\boldsymbol{z}} = -Q[u_r', u_\theta', 0]^T - Q[r^{-1}\partial_\theta \Psi, -\partial_r \Psi, 0]^T. \tag{3.4}$$

The first term on the right-hand side is directly proportional and opposes any flow across the imposed magnetic field lines. Axial flow is unaffected by the Lorentz force. Therefore it is not surprising that the flow pattern is found to elongate in this direction as the strength of the imposed field increases (Chandrasekhar 1961). Taking the curl of (3.4) gives

$$\nabla \wedge \boldsymbol{L} = Q(\partial_z \boldsymbol{u} \wedge \hat{\boldsymbol{z}} - \omega_z' \hat{\boldsymbol{z}}) - Q(\nabla \partial_z \Psi - \omega_z' \hat{\boldsymbol{z}}). \tag{3.5}$$

The ω_z'-terms on the right-hand side of (3.4) cancel. It is well known that components of vorticity perpendicular to an imposed field are preferentially damped. The vorticity of the underlying circular-Couette flow (CCF) points in the z-direction, so CCF is unaffected by the imposed magnetic field, and the effective viscosity of the fluid is unchanged by its presence until the appearance of the Taylor instability.

Taking the dot-product of $\boldsymbol{u}'$ with (2.7a) and integrating over the volume gives an energy balance equation for the disturbance. The nonlinear term

$$\int \boldsymbol{u}' \cdot (\boldsymbol{u}' \cdot \nabla)\boldsymbol{u}' \, \mathrm{d}V = \frac{1}{2} \int \nabla \cdot (u'^2 \boldsymbol{u}') \, \mathrm{d}V \tag{3.6}$$

vanishes due to the boundary conditions. This term represents the transfer of energy within the disturbance to higher modes (smaller length scales) by advection. Using the property

$$\int \boldsymbol{u}' \cdot \nabla^2 \boldsymbol{u}' \, \mathrm{d}V = \int \nabla \cdot (\boldsymbol{u}' \wedge \boldsymbol{\omega}') \, \mathrm{d}V - \int \boldsymbol{\omega}' \cdot \boldsymbol{\omega}' \, \mathrm{d}V, \tag{3.7}$$

where similarly the divergence integral vanishes, the change in kinetic energy can be written as

$$\tfrac{1}{2}\partial_t \int \boldsymbol{u}' \cdot \boldsymbol{u}' \, \mathrm{d}V = \int u_r' u_\theta' \left(\frac{1}{r} - \partial_r\right) \tilde{u}_\theta \, \mathrm{d}V - \int \boldsymbol{\omega}' \cdot \boldsymbol{\omega}' \, \mathrm{d}V - Q \int (u_r'^2 + u_\theta'^2 - u_\theta' \, \partial_r \Psi) \, \mathrm{d}V. \tag{3.8}$$

As the instability that first appears is initially axisymmetric, azimuthal derivatives have been ignored in (3.8). For a steady-state solution the terms on the right-hand side must balance, hence these three terms can be identified as

$$E_1 - E_2 - E_3 = 0. \tag{3.9}$$

The first term, E_1, is the supply of energy to the disturbance from radial shear of the circular-Couette flow. The second term, E_2, is the viscous dissipation and the third, E_3, is the magnetic damping term.

https://doi.org/10.1017/S0022112002002409 Published online by Cambridge University Press

4. Stability of CCF in a weak magnetic field

The linear stability of this flow at various radius ratios (Soundalgekar, Ali & Takhar 1994), for co- and counter-rotating cylinders (Chen & Chang 1998), and at asymptotically large Q (Chandrasekhar 1961), is a well-studied topic, so we focus briefly on the behaviour at small Q. In this and the following sections we find that the magnetic field needs only to be $O(10)$ in order to have a significant affect. By experimental standards this Q is not very large; experiments with $Q > 10^3$ were performed by Donnelly & Ozima (1962).

The disturbance to the CCF can be decomposed into Fourier modes,

$$\boldsymbol{u}'(r,z) = \frac{1}{\sqrt{2}}\boldsymbol{u}'_0(r) + \sum_{k=1}^{\infty} \boldsymbol{u}'_k(r)\cos\alpha k z, \tag{4.1}$$

where $2\pi/\alpha$ is the critical wavelength at which the fundamental disturbance ($k = 1$) first appears. Due to orthogonality of the cosine function we have

$$\frac{1}{2}\int \boldsymbol{u}'\cdot\boldsymbol{u}'\,\mathrm{d}V = \frac{\pi^2}{\alpha}\sum_k \int \boldsymbol{u}'_k\cdot\boldsymbol{u}'_k r\,\mathrm{d}r, \tag{4.2}$$

which allows us to consider the contribution of each mode to the energy.

For a disturbance to the fundamental mode of infinitesimal amplitude A_1, the nonlinear term (3.6) will be very small and modes $k > 1$ can be assumed negligible. At the critical Reynolds number this disturbance neither grows nor decays and can be considered in isolation.

With a fixed outer cylinder the energy, E_1, supplied to the fundamental disturbance is proportional to Re_1, the driving imposed by the inner cylinder. The inviscid Rayleigh criterion predicts that the flow is unstable for any rotation of the inner cylinder. The viscous dissipation, E_2, prevents the immediate onset of TVF. It originates from shears within, and so derivatives of, the disturbance. From (3.8) and (4.1) for the first mode, it is expected that $E_2 = O(\alpha^2 A_1^2)$. For a weak magnetic field the magnetic damping, E_3, is $O(QA_1^2)$, linearly proportional to Q. Provided that the magnetic field is not large enough to affect the wavenumber of the flow, we expect that the critical driving, Re_c, at which the instability first appears, to be delayed linearly with Q. Further, since $\alpha \approx 3$ for hydrodynamic flows, if $Q = O(10)$ then E_2 and E_3 are expected to be of comparable size.

Results of calculations at radius ratios $\eta = 0.65, 0.72, 0.83$ are given in figure 1. The wavenumber decreases approximately linearly by 15% over the not small range of Q in the figure. For each η the wavenumber $\alpha = 3.13, 2.93, 2.70 \pm 0.01$ at $Q = 0, 15, 30$ respectively. The delay of transition to Taylor-vortex flow (TVF) remains almost linear in Q. In the limit $Q \to 0$ we find that $Re_c(Q)/Re_c(0) = 1 + \gamma Q$ where $\gamma \approx 0.0181$ for all η in figure 1. As no energy is passed to higher modes for very small A_1, the structure of the disturbance does not change appreciably with Q or η. Therefore the ratio of magnetic to viscous dissipation remains the same with different η.

5. Nonlinear axisymmetric TVF

In this section we study the nonlinear flows that occur above the first transition. If the inner cylinder is driven past the critical rate, then energy is quickly transferred to higher modes by the nonlinear advection. Isolating one of these modes, the dissipative terms are $E_2 = O(\alpha^2 k^2 A_k^2)$ and $E_3 = O(\gamma Q A_k^2)$. Viscous dissipation quickly becomes

https://doi.org/10.1017/S0022112002002409 Published online by Cambridge University Press

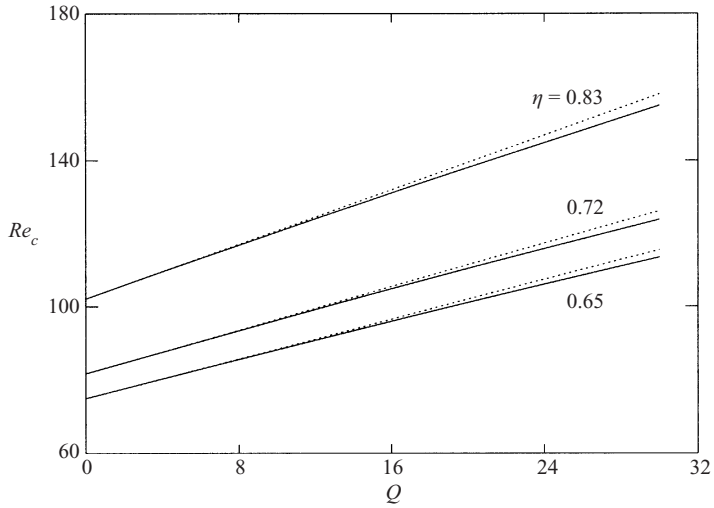


FIGURE 1. Delay of onset of TVF by an imposed axial field. Dotted lines are linear extrapolations from Q small.

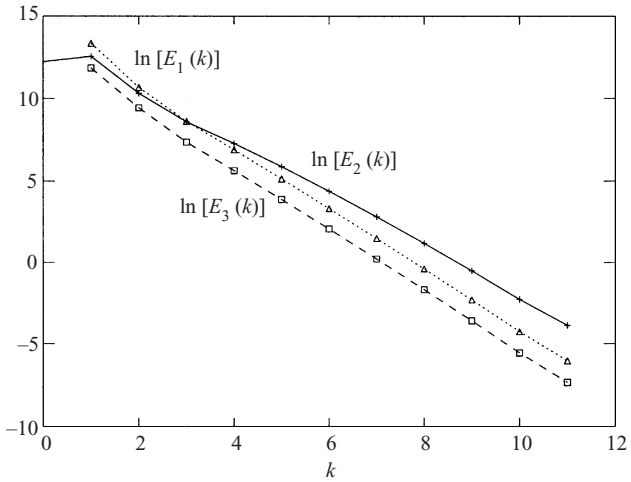


FIGURE 2. Typical spectrum of energy terms. For the first few modes magnetic (dashed) and viscous (solid) dissipations are comparable. Viscous dissipation dominates the behaviour of higher modes, and $E_2/E_3 \propto k^2$. ($Q = 30$, $\eta = 0.65$, $\alpha = 2.71$, $Re_1 = 1.5Re_c$, $Re_c = 113.4$.)

dominant as energy moves to higher modes. This can be seen in figure 2. However, magnetic damping remains significant for the fundamental mode, draining energy before it can be passed to higher wavenumbers. There the fluid viscosity determines the amplitude of the disturbance. The net result can be seen in figure 3 where we plot the amplitude of the disturbance at different values of Q. A relatively wide gap, $\eta = 0.65$, was chosen for the calculations, as the axisymmetric flow is stable to non-axisymmetric perturbations well beyond the onset of TVF. The maximum axial velocity, rather than the radial velocity, was used to characterize the amplitude of nonlinear TVF, as the outflow becomes increasingly jet-like as Re_1 is increased. Tabeling (1981) used an amplitude expansion about the point of criticality in the narrow gap limit to show that in the weakly nonlinear regime $A \propto \beta(Re_1 - Re_c)^{1/2}$, and

https://doi.org/10.1017/S0022112002002409 Published online by Cambridge University Press

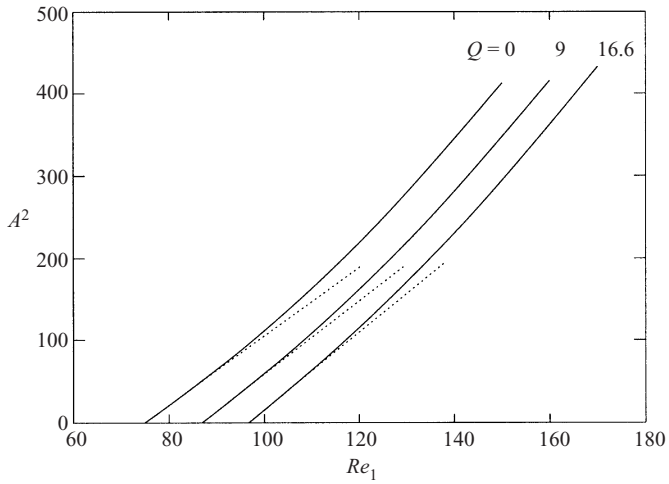


FIGURE 3. Square of maximum axial velocity versus Re_1 in the presence of imposed axial magnetic fields. $\eta = 0.65$.

that β does not strongly depend on Q. From figure 3 we see that this approximation is valid well beyond the critical point, even though the nonlinearity affects the flow pattern.

Kikura, Takeda & Durst (1999) performed experiments to measure fluid velocities in nonlinear hydromagnetic flow. Their imposed field was different from ours, so we cannot make a direct quantitative comparison. However, the same order-of-magnitude arguments for the energy of the harmonics still hold, and the numerical results presented in this section are qualitatively the same as their experimental results.

Since the magnetic damping is effective only on larger length scales, apart from a change in wavelength of the flow, the flow pattern of nonlinear axisymmetric TVF in the presence of an imposed axial field is very similar to that in the hydrodynamic (non-magnetic) case. This is apparent from figure 3 where the main difference is only that the onset of TVF is delayed. This can also be seen in figure 4 where $(Re_1 - Re_c(Q))$ is the same for both plots (with $\eta = 0.83$, and (a) $Q = 0$, $Re_1 = 1.5Re_c(0)$, $\alpha = 3.13$; (b) $Q = 20$, $Re_1 = Re_c(Q) + 0.5Re_c(0)$, $\alpha = 2.85$). Although the axial wavelengths differ, both are plotted the same size for comparison. The azimuthal flow is faster than CCF ($u'_\theta > 0$) in the outflow regions ($z = \pi/\alpha$) and slower ($u'_\theta < 0$) in the inflow regions ($z = 0, 2\pi/\alpha$). The only clear observable difference is that the fast azimuthal jet-flow region that occurs at the outflow is slightly larger for the magnetic flow, in addition to the stretched axial wavelength. However, figure 4(b) is almost indistinguishable from hydrodynamic flow at the longer wavelength, $\alpha = 2.85$, where $Re_1 = 1.5Re_c$ (not plotted). The deviation from CCF is large; the maximum of u'_θ is approximately 35% of the maximum of $\tilde{u}_\theta = Re_1$. The maximum values of $|u'_{r,\theta,z}|$ for all three sets of parameters are within 2%, except for $|u'_z|$ in the magnetic flow which is 8% larger. The Lorentz force has no z-component and so does not damp axial flow, and therefore the curves in figure 3 are not quite parallel. Despite only small differences in the flow patterns, only the magnetic flow is stable to non-axisymmetric disturbances, which is the topic of the next section.

6. The transition to wavy flow

Finding the preferred mode and transitions between fully developed nonlinear wavy modes is an enormous challenge. For the sake of simplicity, we investigate

https://doi.org/10.1017/S0022112002002409 Published online by Cambridge University Press

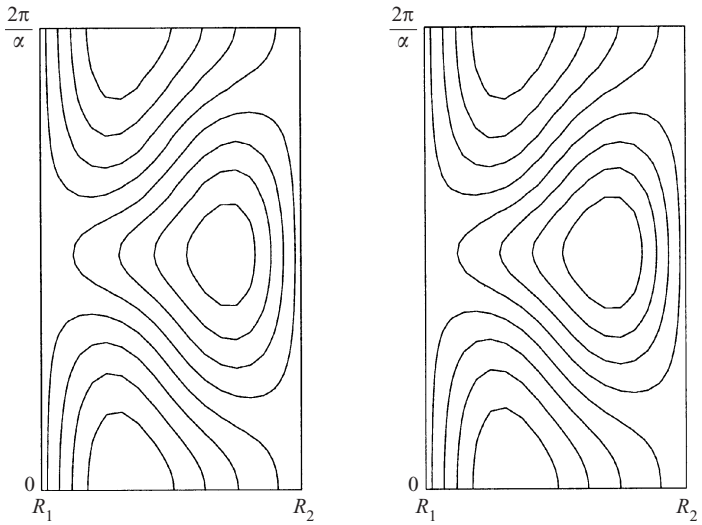


FIGURE 4. Contours of u'_θ at $\eta = 0.83$ for (a) $Q = 0$, $Re_1 = 1.5Re_c(Q = 0)$, $\alpha = 3.13$ and (b) $Q = 20$, $Re_1 = Re_c(Q) + 0.5Re_c(0)$, $\alpha = 2.85$.

which modes are possible by monitoring the growth or decay of infinitesimal non-axisymmetric disturbances to the axisymmetric TVF. The disturbance translates in the azimuthal direction at some fraction of the rotation rate of the inner cylinder – the wave speed s.

In the hydrodynamic case, Jones (1985) calculated stability boundaries and corresponding wave speeds by solving the eigenvalue problem. The stability of axisymmetric flow was found to depend strongly on the radius ratio. Figure 5 shows the stability boundaries and corresponding wave speeds at onset of the wavy modes. The stability boundaries are shown relative to Re_c for the onset of TVF ($m = 0$). For increasing Reynolds numbers and $\eta > 0.75$, we see that TVF can be destabilized to the $m = 1$ wavy mode (lower part of the boundary in figure 5a) and then be restabilized by a further increase of the Reynolds number (upper part of the boundary). Such transition sequences predicted by Jones' results were verified experimentally by Park & Jeong (1984).

The critical Reynolds number for the disappearance of $m = 1, 2$ modes (upper boundary) increases rather rapidly as η is increased past about 0.85. Therefore the choice $\eta = 0.83$ was taken for our magnetic calculations.

The magnetic field, imposed axially, has the effect of increasing the critical wavelength for onset of TVF. Jones (1985) held α fixed at 3.13, but this becomes inappropriate for our magnetic calculations. Figure 6 shows the stability of the equilibrated TVF that appears at the critical wavenumber for the given field strength, $\alpha(Q)$. The dotted lines are the stability boundaries for bifurcation from CCF, as calculated by Chen & Chang (1998). The difference between the dotted lines and the solid lines confirm Jones' assertion that it is essential to perturb TVF (which must be computed numerically) to understand the onset of wavy modes. The stability boundaries for the onset of wavy modes are sensitive to small differences in the parameters, and the magnetic field does not need to be strong to produce interesting effects.

The magnetic damping term in (3.8) damps the radial and azimuthal components of the axisymmetric flow. The curvature of the cylinders also has an additional effect

https://doi.org/10.1017/S0022112002002409 Published online by Cambridge University Press

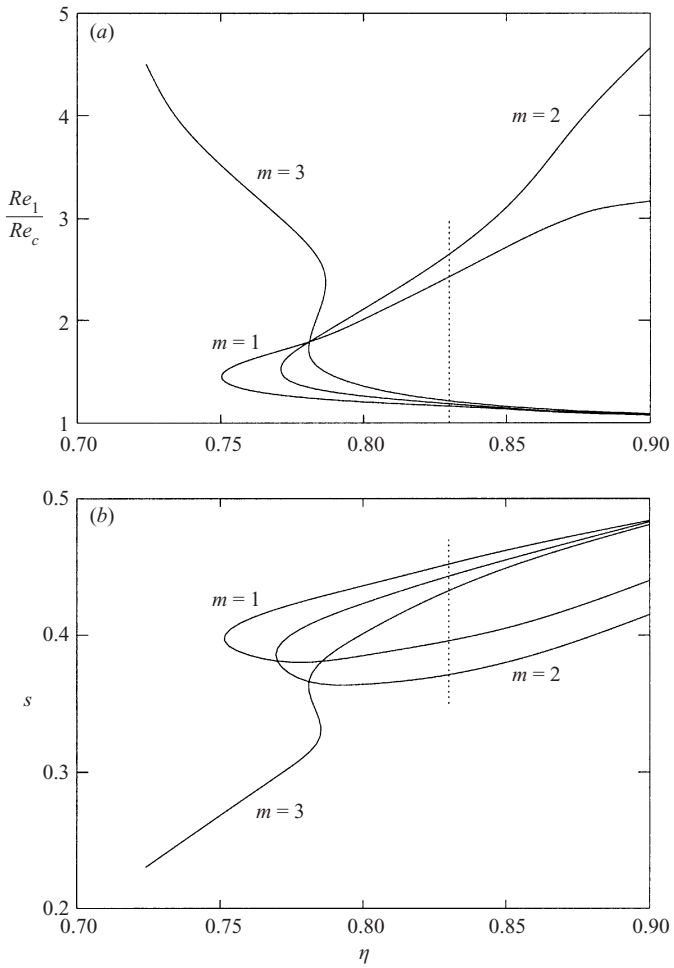


FIGURE 5. (*a*) Stability of axisymmetric TVF to non-axisymmetric perturbations over a range of η, as determined by Jones (1985), $\alpha = 3.13$. (*b*) Corresponding wave speeds, s, at onset as a fraction of Ω_1. The dotted line is the intersection with the magnetic results at $\eta = 0.83$.

on the viscous dissipation of these two components of the velocity. There is a clear similarity between increasing the imposed magnetic field strength and decreasing the radius ratio. We do not pursue this relationship very far as the stability boundaries have not been fully explained, even for hydrodynamic flows. However, significant progress on the mechanism involved was made by Jones (1985).

Jones (1985) noted that dissipation due to the radial and axial shear within TVF appears to be an important factor in the stability of the azimuthal jet that appears at the in- and outflows. The elongation of Taylor cells over the range of Q in figure 6 (by around 10%) might be a factor in the suppression of wavy modes. Antonijoan & Sánchez (2002) investigated the hydrodynamic stability to wavy modes as a function of α. The resulting stability boundaries are qualitatively similar to figure 6(*a*) for increasing wavelength. However, from the results of Antonijoan & Sánchez (2002), the change in α over the range for Q in figure 6(*a*) is a factor of 2–3 smaller than that required to suppress only the $m = 1$ mode. The enhanced stability must also be attributed to magnetic damping of the disturbance.

https://doi.org/10.1017/S0022112002002409 Published online by Cambridge University Press

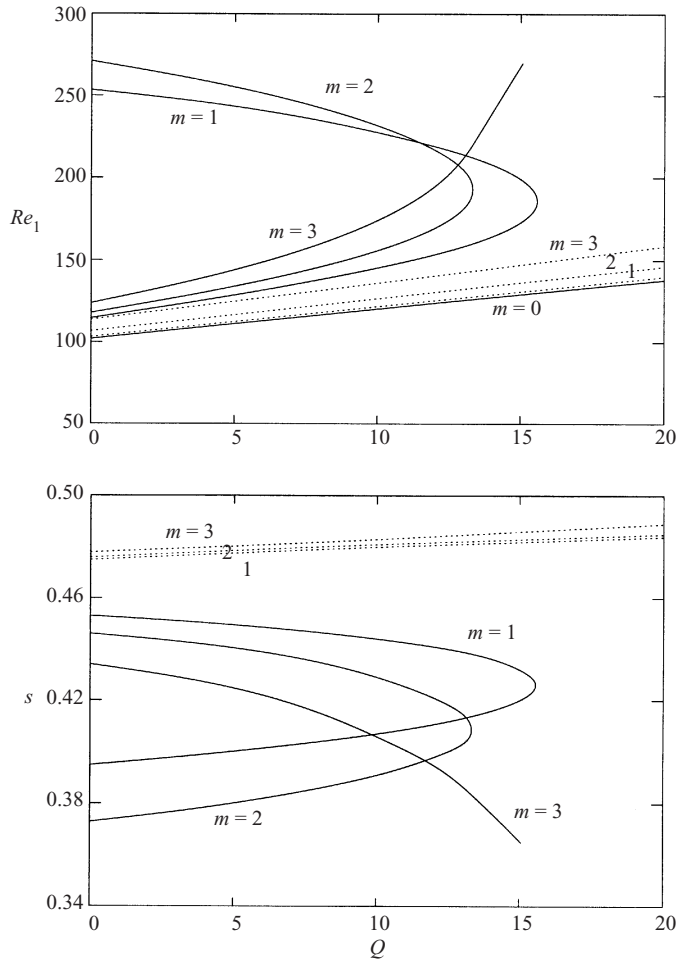


FIGURE 6. For $\eta = 0.83$, $\alpha = \alpha_c(Q)$: (a) stability of hydromagnetic TVF to non-axisymmetric perturbations for increasing magnetic field strength, and (b) corresponding wave speeds at onset. Dotted lines are bifurcations from CCF.

The general trend in figure 5(b) is for the wave speed, s, to decrease with decreasing η. For wider gaps there is more fluid in the slower outer regions and the mean azimuthal flow speed decreases with increasing gap width, as does s. Also, as the Reynolds number is increased the outflow region narrows and the inflow region becomes larger than that of the outflow. Therefore the bulk of the fluid is in the slower inflow region and again the mean azimuthal flow is reduced. This mean-flow interpretation of the wave speed is consistent with the findings in figure 6(b). Here the wave speed decreases with increasing Reynolds number, as the outflow still narrows and the inflow broadens, but the gap width is fixed and there is no additional decrease in the pattern when the magnetic field strength increases. Compare figure 5(b) for decreasing η with figure 6(b) for increasing Q.

7. Conclusions

We have investigated magnetic Taylor–Couette flow in the nonlinear regime. In the presence of an imposed axial magnetic field the Lorentz force is found to have a

https://doi.org/10.1017/S0022112002002409 Published online by Cambridge University Press

significant damping affect, but only at larger length scales. This is a consequence of the small magnetic Prandtl number limit, relevant to experiments with liquid metals, for which the magnetic field is completely defined by the velocity field.

When the imposed field is not too large, the axial wavenumber of the flow is not greatly affected. In this weak-field regime the stability of circular-Couette flow is enhanced linearly with Q, $Re_c(Q)/Re_c(0) = 1+\gamma Q$ where γ appears to be independent of the gap width.

In the nonlinear regime, magnetic damping affects disturbances at the fundamental axial wavenumber, but the remaining energy passed to higher modes is dissipated mainly by the fluid viscosity. This determines the amplitude of the disturbance, which behaves approximately like $\beta(Re_1 - Re_c(Q))^{1/2}$ well beyond the critical point, where β does not depend strongly on Q. This is consistent with the findings of the amplitude expansion by Tabeling (1981).

Our main finding is that the magnetic field has its most striking effect on the stability of TVF to wavy modes. A small field is capable of pushing the secondary instability from only a few percent above the first instability to several times the critical Reynolds number for the onset of TVF. This is similar to the relative stability of TVF to wavy perturbations in wide gaps. As in hydrodynamic flows, the wave speed decreases with increased Reynolds number, but the dependence of the wave speed on the imposed field strength does not appear as strong as the dependence on the gap width.

The significant enhanced stability observed in the calculations above occurs at only relatively small imposed field strengths, well within the experimental range. As a secondary bifurcation, the transition to wavy modes is difficult to detect accurately via torque measurements. A visualization technique, using ultrasound, is being developed for opaque fluids by Kikura *et al.* (1999). This type of transition could serve as a good test for flow visualization in magnetic fluids, where the transitions are accurately defined. The new technique is of particular interest to those working on dynamo experiments.

The authors wish to thank Professor Chris Jones for helpful comments and suggestions during this work.

REFERENCES

Andereck, C. D., Liu, S. S. & Swinney H. L. 1986 Flow regimes in a circular Couette system with independently rotating cylinders. *J. Fluid Mech.* **164**, 155–183.

Antonijoan, J. & Sánchez, J. 2002 On stable Taylor vortices above the transition to wavy vortices. *Phys. Fluids* **14**, 1661–1665.

Chandrasekhar, S. 1961 *Hydrodynamic and Hydromagnetic Stability*. Clarendon.

Chen, F. & Chang, M. H. 1998 Stability of hydromagnetic dissipative Couette flow with non-axisymmetric disturbance. *J. Fluid Mech.* **366**, 135–158.

Donnelly, R. J. & Ozima, M. 1962 Experiments on the stability of flow between rotating cylinders in the presence of a magnetic field. *Proc. R. Soc. Lond.* A **226**, 272–286.

Egbers, C. & Pfister, G. 2000 *Physics of Rotating Fluids*. Springer.

Gailitis, A., Lielausis, O., Platacis, E., Dement'ev, S., Cifersons, A., Gerbeth, G., Gundrum, T., Stefani, F., Christen, M. & Gotthard, W. 2001 Magnetic field saturation in the Riga dynamo experiment. *Phys. Rev. Lett.* **86**, 3024–3027.

Hollerbach, R. & Skinner, S. 2001 Instabilities of magnetically induced shear layers and jets. *Proc. R. Soc. Lond.* A **457**, 785–802.

Ji, H., Goodman, J. & Kageyama, A. 2001 Magnetorotational instability in a rotating liquid metal annulus. *Mon. Not. R. Astron. Soc.* **325**, L1–L5.

https://doi.org/10.1017/S0022112002002409 Published online by Cambridge University Press

Jones, C. A. 1985 The transition to wavy Taylor vortices. *J. Fluid Mech.* **157**, 135–162.

Kikura, H., Takeda, Y. & Durst, F. 1999 Velocity profile measurement of the Taylor vortex flow of a magnetic fluid using the ultrasonic Doppler method. *Exps. Fluids* **26**, 208–214.

Park, K. & Jeong, K. 1984 Stability boundary of the Taylor vortex flow. *Phys. Fluids* **27**, 2201–2203.

Rüdiger, G. & Zhang, Y. 2001 MHD instability in differentially-rotating cylindric flows. *Astron. Astrophys.* **378**, 302–308.

Soundalgekar, V. M., Ali, M. A. & Takhar, H. S. 1994 Hydromagnetic stability of dissipative Couette flow: wide-gap problem. *Int. J. Energ. Res.* **18**, 689–695.

Stieglitz, R. & Müller, U. 2001 Experimental demonstration of a homogeneous two-scale dynamo. *Phys. Fluids* **13**, 561–564.

Tabeling, P. 1981 Magnetohydrodynamic Taylor vortex flows. *J. Fluid Mech.* **112**, 329–345.

Taylor, G. I. 1923 Stability of a viscous liquid contained between two rotating cylinders. *Phil. Trans. R. Soc. Lond.* A **223**, 289–343.

Willis, A. P. & Barenghi C. F. 2002 Hydromagnetic Taylor–Couette flow: numerical formulation and comparison with experiment. *J. Fluid Mech.* **463**, 361–375.

https://doi.org/10.1017/S0022112002002409 Published online by Cambridge University Press